Preprint Title	Analysis of catalyst surface wetting: the early stage of epitaxial germanium nanowire growth
Authors	Owen C. Ernst, Felix Lange, David Uebel, Thomas Teubner and Torsten Boeck
Publication Date	18 Jun 2020
Article Type	Full Research Paper
Supporting Information File 1	Appendix_Ernst er al_Analysis of catalyst surface wetting_the early stage of epitaxial germanium nanowire growth.docx; 28.2 KB
ORCID® iDs	Owen C. Ernst - https://orcid.org/0000-0003-1429-9763; David Uebel - https://orcid.org/0000-0003-4066-5691; Thomas Teubner - https://orcid.org/0000-0001-8132-7301

Analysis of catalyst surface wetting: the early stage of epitaxial germanium nanowire growth

Owen C. Ernst,* Felix Lange, David Uebel, Thomas Teubner and Torsten Boeck

Adress: Leibniz-Institut für Kristallzüchtung, Max-Born-Straße 2, 12489 Berlin, Germany
Email: Owen C. Ernst – owen.ernst@ikz-berlin.de
* Corresponding author

Abstract

In several nanotechnological applications the dewetting process is crucial. Although not all phenomena of dewetting are fully understood yet, especially with regard to metallic fluids, it is clear that the formation of nanoparticles, -droplets, and -clusters and their movement is strongly linked to their wetting behaviour. For this reason, the thermodynamic stability of thin metal layers (0.1 – 100 nm) with respect to its free energy is examined here. The decisive factor for the theoretical consideration is the interfacial energy. In order to achieve a better understanding of the interface interactions, three different models for the estimation of this energy are presented: i. fully theoretical, ii. empirical and iii. semi-empirical. The formation of nanometre-sized gold particles on silicon and silicon oxide is investigated in detail, elucidating the strengths and weaknesses of the three models, comparing the different substrates, and verifying the possibility of further processing of the gained particles as nanocatalysts. The importance of a persistent thin communication wetting layer between the particles and its effects on their size and number also becomes clear. In particular, the intrinsic reduction of the Laplace pressure of the system by material re-evaporation and Ostwald ripening is considered to describe the theoretically predicted and experimentally found effects. Thus dewetting phenomena of thin metal layers can be well-directed used for the manufacturing of nanostructured devices. From this viewpoint, the behaviour of gold droplets as catalysts to grow germanium nanowires on different substrates is described.

Introduction

Wetting phenomena and the formation and movement of droplets are essential for numerous applications. Surface treatments, for example, modify the wetting behavior of active fluids on composite materials or porous media to increase the efficiency and selectivity of catalytic processes.[1] Droplet-based microfluidics, which deals among other things with on-chip and off-chip incubation in immiscible phases even developed into an independent field of science.[2] This shows that wetting phenomena are crucial for a variety of industrial processes and research topics, as well. In microtechnology, the dispersion of organic photoresists on substrates is indispensable for lithographic top-down microstructuring to produce highly functional intermediate products for further processing.[3][4] However, the presence of droplets and dewetting phenomena are not only observed in aqueous and organic systems, but in inorganic systems, such as liquid metals[5] or (ultra-)thin layers[6], too. The formation of metallic nanodroplets can be favourable when intentionally used, e.g. to create strongly localized heat sources[7][8], but can be disruptive, such as in the case of the collapse of ultra-thin copper layers on titanium nitride which damages the electronic devices.[9][10] However, these phenomena in thin film technologies are rarely attributed to the dewetting process, which is recognizable in the usual naming of the resulting structures as nanoparticles or clusters but only infrequently as droplets. Nevertheless, the origin of these structures from fluid-like states offers the opportunity for novel bottom-up techniques to produce precursor materials for functional materials such as chalcopyrites[11] or precursors for complex structures such as nanowires.[12] Silicon, germanium and silicon oxide nanowires, for example, can be formed on different substrates using metal catalysts in form of tin, indium or gold nanodroplets.[13][14] Such nanometre-sized one-dimensional materials are therefore promising for gate all-round architectures[15], which are very attractive for future low-power field effect transistors (FETs)[16] or thermoelectrics.[17][18][19]

The formation of nanodroplets as described leads to various outcomes depending on the combination of substrate and droplet material. Thus, the interactions between the catalytic nanodroplets and the substrate surface must be investigated in more detail beforehand to gain a better understanding and control over the process. The examination of the surface diffusion processes was carried out here to describe the growth process, in order to effectively control the formation of the nanostructures.

As an example of various metallic droplet interactions with diverse surfaces the behaviour of gold deposited on silicon and silicon oxide wafers is demonstrated. The property of gold to form a layer, droplets or particles on silicon or silicon oxide is theoretically described and experimentally shown by ultra-high vacuum physical vapour deposition (UHV-PVD) of the predicted structures. The theoretical description base on a fundamental description of the dewetting phenomenon from an energetic point of view. A closer look is taken at the thermodynamic differences in free energy and interfacial potentials between gold and silicon or silicon oxide. For this purpose, the interfacial potentials are calculated using three different techniques: An empirical approach in which the **w**etting **a**ngle is taken into account (**WA model**); a completely theoretical approach in which the interface is described only by **v**an der **W**aals interactions (**vW model**); and a semi-empirical approach in which R. H. Ewing's considerations of the interface energy between a solid metal and its own melt are applied to a substrate-fluid interface of different materials (**AE model**). The influence of the resulting free energy leads to differently pronounced nanodroplets and changes their behaviour as catalysts during the growth of nanowires which is shown in the following.

Results

Theoretical Results

Gold on silicon oxide – Au on SiO_x

Figure 1 shows the first derivative of the free energy to the layer thickness. Two different behaviours of gold on silicon oxide depending on the used model can be seen. While the vW model has a zero crossing in d_{real} = 0.5 nm, the other two models follow a classical dewetting mechanism: The function of the first derivative only assumes values below the abscissa axis and converges towards zero. This is a major difference since values above zero lead to the formation of a continuous thin film. Respectively, values below zero promote the formation of droplets on the surface.

Since a monolayer of gold has a nominal thickness of 0.32 nm, the maximum thickness of 0.5 nm predicted in vW-model is already exceeded with a second monolayer of gold. Consequently, this model predicts the layer growth of gold on silicon oxide. In contrast to the vW model, the other two models WA and AE predict droplet formation over the entire thickness range.

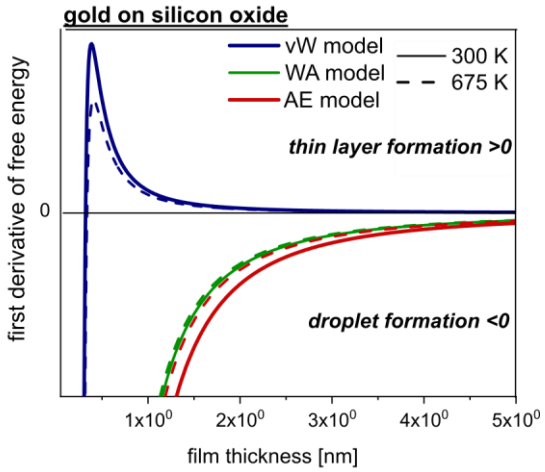

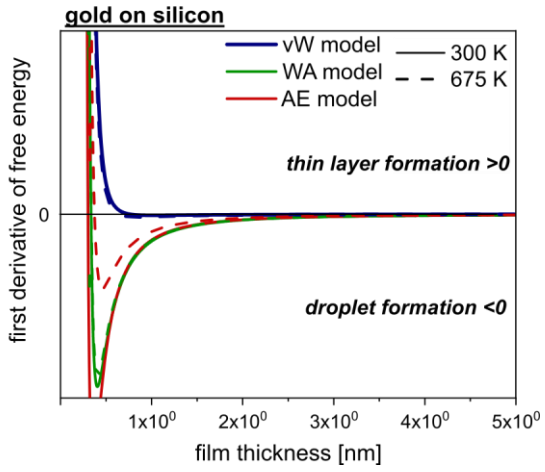

Figure 1: Derivative of the free energy versus the film thickness for gold on silicon oxide and gold on silicon at 300 K (solid lines) and 675 K (dashed lines). The calculations for the interfacial energy was made by three different models vW (bluei), WA (green) and AE (red). Values above zero indicate a stable thin layer of gold, while values below zero indicate an unstable thin layer, which consequently results into the formation of droplets or particles.

Gold on silicon – Au on Si

In contrast to gold on silicon oxide, gold on silicon in figure 1 shows a dependence of the free energy on temperature. As the temperature rises, the first derivative of the free energy, respectively its slope, increases. Qualitatively, all three models predict the same behaviour: Gold forms droplets on silicon with a wetting layer between the droplets. The thickness of the wetting layer lays between 0.37 nm and 0.49 nm at room temperature and between 0.42 nm and 0.71 nm at 400° C, since the zero crossings of the graphs arise at these values. Assuming a monolayer thickness of gold of 0.32 nm, one or two monolayers of gold at room temperature and one to three monolayers at 400°C are stable, as long as the systems are in thermodynamic equilibrium

Practical Results

Gold on silicon oxide – Au on SiO_x

UHV-PVD deposited gold droplets on SiO_x are characterized in figure 2. Here the behaviour of mean gold droplet diameter and the number of gold droplets per area over substrate temperature are shown both. The size distribution at 300°C is also presented, which is representative for all distributions in the temperature range shown. The diameter of the gold droplets remains constant throughout, while the size distribution can be described by a Gaussian distribution curve. In the visualization of the number of droplets per area two temperature ranges are visible which merge into each other at

approximately 550° C. At this point the number of droplets is minimal and increases with rising distance from this point.

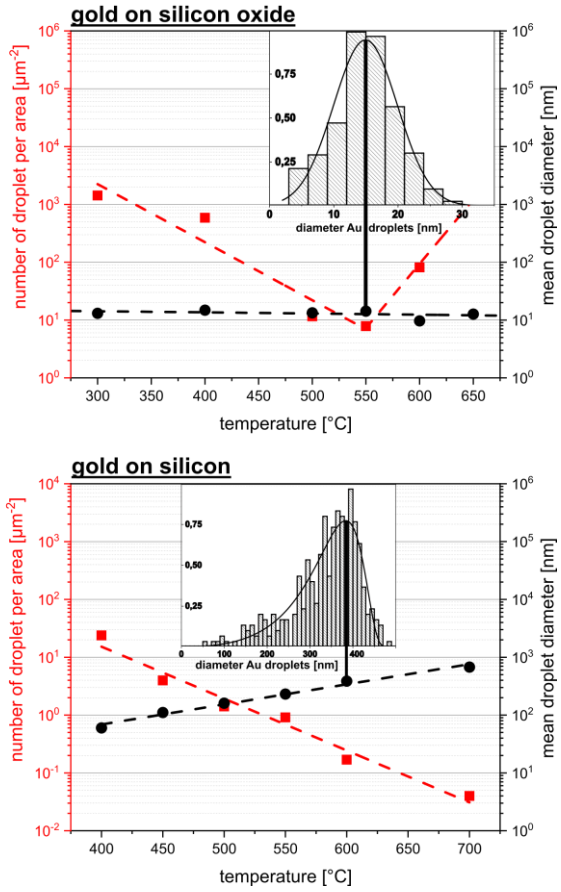

Figure 2: Behaviour of gold droplets on silicon oxide and silicon. The plots show the evolution of the number of droplet per area (red squares, guide to the eye: red dashed line) and mean droplet diameters (black dots, guide to the eye: black dashed line) with respect to the substrate temperature. The insets show histograms containing the size distribution of droplet diameters at 550°C (Au on SiO_x) and at 600°C (Au on Si). For Au on SiO_x the distribution is approximated by a Gaussian. For Au on Si the distribution is given by a Lifshitz-Slyosov-Wagner expression.

Gold on silicon – Au on Si

In figure 2 also results for gold droplet formation on Si(111) wafers are shown. A decrease in number and an increase in droplet diameter with temperature can be seen. The droplet diameter distribution shown can be described by a Lifshitz-Slyozov-Wagner (LSW) distribution. Figure 3 shows gold particles on silicon at room temperature. Tiny

gold clusters of less than 10 nm are visible between the droplets in the SEM and the TEM image.

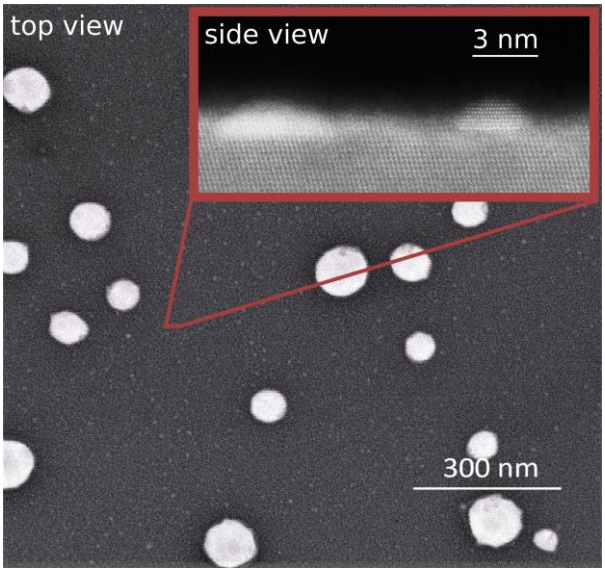

Figure 3: SEM image of gold on silicon after cooling down to room temperature. Between the droplets tiny clusters of gold have nucleated on the silicon surface. The inset shows a TEM image of those tiny gold clusters.

Growth of germanium nanowires

Figure 4 shows images of the resulting gold droplets on various substrates and the results after deposition of germanium on these samples. In (a) a silicon oxide substrate was used for gold deposition. In (b) the sample was deposited with germanium. No 1D structures are formed here. Instead, there are random germanium clusters everywhere on the sample. (c) and (d) show the results for gold deposition and subsequent germanium deposition on silicon. Here the gold droplets are much greater than on silicon and germanium nanowires were grown. The in-plane nanowires started to grow at places where the gold droplets formed before. The inset shows that the gold is still on top of the wire, as this is where continuous homoepitaxial growth is catalysed. A sample with a silicon nanotip[20] surrounded by a silicon oxide matrix is shown in (e) and (f). The gold droplet forms on the silicon tip during gold deposition. After germanium

deposition, the gold droplet on the silicon tip forms a single in-plane nanowire on the surface of the silicon oxide matrix.

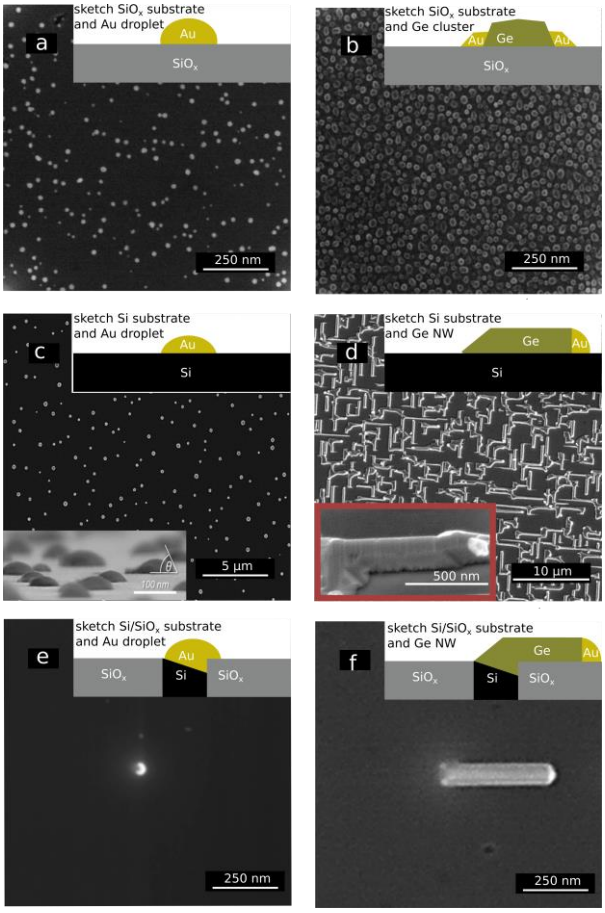

Figure 4: Images of the gold droplets and the results after the experiments to grow germanium nanowires. The insets at the upper right corners show sketches of the shown systems in side view. a: SEM top view image of gold nanodroplets (≈15 nm) on silicon oxide. b: SEM image of a gold/silicon oxide sample after germanium deposition. The growth of nanowires was not catalysed by the gold droplets. Instead, germanium clusters are formed. c: SEM top view of gold nanodroplets (≈100 nm) on silicon. The inset at the lower left corner shows an image of an inclined sample with a drawn-in wetting angle θ. d: SEM image of germanium-1D structures on germanium, which are formed by the gold droplets catalysed during germanium deposition. The inset at the lower left corner shows an image of an inclined sample. The droplet on top of the wire is clearly visible. e: SEM top view of one gold nanodroplet on a silicon tip in a silicon

oxide matrix. As can be seen, the droplet sits on only one side of the silicon tip. f: SEM image of the sample shown in e after germanium deposition. The drop catalysed the growth of a nanowire.

Discussion

The aim of this publication is a two-fold insight. Firstly, the comparison the three different models of interfacial energy and their agreement with the experimental results (Table 1). Secondly, the behaviour of gold on silicon oxide and gold on silicon will be compared.

Gold on silicon oxide – Au on SiO_x

The two models WA and AE show that a thin gold layer on silicon oxide is unstable and therefore forms droplets or particles on the surface (figure 1). Only the fully theoretical VW model for the interfacial energy predicts a free energy which leads to a stable thin gold layer for thicknesses above 0.5 nm. But the experimental data, as shown in figure 2, 3, and 4, indicate that the vW model fails here due to the clear observable formation of gold droplets on the silicon oxide surface. Calculations by van-der-Waals interactions need a deep insight into characteristics and properties of the observed material. But in thermal silicon oxide there is no defined crystallographic orientation and no defined surface chemistry, since different types of oxide can occur. The complete theoretical description of gold on silicon oxide by the vW model fails because there is not enough information about this morphologically and chemically heterogeneous silicon oxide surface. Even for thermal silicon oxide surfaces which have grown in a well-controlled process, only approximate values are given in the literature.[21] In addition, the van der Waals energy between silicon oxide and gold is repulsive, which is unsuitable for a model that assumes two surfaces, that are brought closer together. For such complex and repulsive systems, empirical or semi-empirical methods are more appropriate.

model (abbreviation)	WA	vW	AE
name	wetting angle	van der Waals	approaching to R.H. Ewing
formula for the interfacial energy	eq. (5)	eq. (7)	eq. (8)
formula for the resulting free energy	eq. (9)	eq. (10)	eq. (11)
approach	emperical	theoritical	semi-emperical
short description	Wetting angles between substrate and droplets are connected to the interfacial energy by the Young-Dupré equation.	The interfacial energy is related to the polarizabilities of the used materials. This can be estimated by the long range contribution of van der Waals energy	The interfacial energy between a solid and a fluid consists of two parts: a solid part and a fluid part. These fractions can be estimated based on material parameters.
assuming nanodroplets of Au on SiOx	yes ✓	no ✗	yes ✓
assuming a wetting layer of Au on SiOx	no ✓	yes ✗	no ✓
assuming nanodroplets of Au on Si	yes ✓	yes ✓	yes ✓
assuming a wetting layer of Au on Si	yes ✓	yes ✓	yes ✓
strengths	high agreement with experimental results simple	no emperical data nedded	high agreement with experimental results little susceptibility to faults
weaknesses	only available for systems with droplet formation hysteresis effects	very susceptible to faults only valid for well-known systems fails for Au on SiOx	requires a high amount of data

✓ - in agreement with experimental results ✗ - not in agreement with experimental results

Table 1: Comparison between the three models WA, vW, and AE and the experimental results.

On silicon oxide, the number of droplets per area of gold decreases up to a temperature of 550°C. At higher temperature the number then rises again. The mean droplet diameter remains constant over the entire temperature range. This effect can be explained by re-evaporation of the droplets. The vapour pressure of bulk gold at 550° C is 10^{-14} - 10^{-16} bar[22] and becomes even higher on surfaces with strong curvature such as droplets. Small droplets are characterized by a high surface curvature, which leads to a high Laplace pressure. As the temperature rises, the Laplace pressure in the droplets increases, increasing the likelihood of re-evaporation as long as the pressure cannot be reduced by other effects such as Ostwald ripening. Ostwald ripening needs a medium of material transport. But since there is no wetting layer according to two models WA and EA in figure 1, this pressure cannot be relieved by Ostwald ripening. Nevertheless, an Ostwald ripening process could also take place through the gas phase, although this process is kinetically inhibited.

The re-evaporation process leads to a decreasing number of droplets per area, while the droplet diameters remain constant and the diameter distribution remains Gaussian, and no LSW distribution as in Ostwald ripening processes.[23][24] This behaviour derived from theoretical considerations fits with the results in figure 2, 3, and 4. The increasing number of droplets above 550°C can be attributed to a spinodal dewetting mechanism: Higher temperatures in the initial fluid layer leads to greater internal heat and faster movements of atoms. Thus the system reaches a supercritical state, in which the layer thickness fluctuates increasingly and finally destabilises. Therefore higher temperatures result in higher numbers of droplets per area during dewetting.

Gold on silicon – Au on Si

All three models show the same behaviour of droplet formation for gold on silicon, which is confirmed in the experiments and described in the literature.[25] This second system is simpler to model than the first system of gold on silicon oxide. Pure silicon wafers have a defined surface orientation with well understood physical and chemical properties, wherefore even the fully theoretical model vW fits the real behaviour.

Nevertheless, the results for gold on silicon also vary due to the wide range of possible Hamaker constants, which are needed in the calculations. Hamaker constants can be found in literature, measured, calculated by material constants (see equation (3)) or simulated by microscopic and macroscopic models. This variety for the determination leads to a wide spectrum of different values. Furthermore only the non-retarded interactions are considered, but at higher thicknesses (> 10 nm) the retarded interactions become more relevant. Nevertheless, all essential effects and values occur in thicknesses below 1 nm. Since the Hamaker constant is a critical value for the models shown here, its wide range can lead to difficulties in obtaining reliable values for the free energy of a system, especially for the fully theoretical model, which focuses on the van der Waals interactions. However, the theoretical predictions for gold on silicon fit very well to the observed experimental behaviour. The theoretical results predict a gold wetting layer on silicon of 0.34 nm. As seen in figure 2, the number of droplets per area of gold decreases with increasing temperature, while the droplet diameter increases. This effect can be linked to the wetting layer. Such a layer acts as a mediating communication layer among the droplets and promotes the material transport, thereby accelerating such effects as Ostwald ripening. This argumentation is also supported by the observed LSW distribution of droplet diameters, hence this distribution is characteristic for Ostwald ripening processes. Nevertheless, it should be mentioned that thicker wetting layers can occur at high temperatures if the system deviates from its equilibrium state. It can therefore be assumed that smaller droplets can form between the larger droplets if the thickness of the wetting layer is forced to decrease during cooling as it is shown in figure 3. Tiny gold clusters of less than 10 nm are visible between the droplets. This indicates that the wetting layer collapses during cooling. It remains unclear whether the wetting layer completely disappears into these clusters or just becomes thinner or perforated. However, the TEM data do not show any evidence of a wetting layer at room temperature, only of the tiny gold clusters that form during the cooling process. This is in high agreement with the LEEM calculations given in the

literature, which predict a change in the surface recombination of gold on silicon formed during cooling.[26]

Growth of germanium nanowires

The main reason for germanium nanowires growing on silicon and not on silicon oxide lays in the size of the gold droplets. Since the nanowire growth by VLS process is a catalytic process there has to be a minimum amount of gold atoms inside the droplet to solve germanium inside the gold cluster. This minimum amount is exceeded on silicon while it is not on silicon oxide. However, in literature there is evidence that wire growth by VLS is possible on silicon oxide, but the gold droplets are generated by a different process and are much larger than in this study. This also strongly indicates a size effect. If there are silicon and silicon oxide areas on a substrate as it is the case in figure 4 (e) and (f), the gold place itself purposefully on the silicon area. Bearing in mind that a eutectic decomposition of gold and silicon takes place in bulk mixtures at a temperature of 630 K a chemical affinity of gold for silicon can be supposed. The chemical affinity of silicon to gold is also indicated by the fact that up to 2 ppm gold can dissolve in bulk silicon at higher temperatures.[22] Therefor the formation of the major droplet on silicon is no effect of Laplace pressure – neither reevaporation nor Ostwald ripening. It is just an effect of compound affinity. The droplet even etches the silicon into a stable <111> plane, which is why the droplet seem to be placed just on one site of the silicon spot. The germanium nanowire then grows from the etched facet in <110> direction.

Conclusion

A theoretical prediction of the behaviour of metal droplets on different surfaces was presented. For this purpose, thin gold layers on silicon oxide and silicon were prepared and investigated. Both systems show the formation of gold droplets or particles on the surface. The theoretical description focuses on the determination of the interfacial energies between gold and silicon oxide and gold and silicon, respectively. Three

models were presented: A fully theoretical model (vW model), a semi-empirical model (AE model) and a fully empirical model (WA model). The interfacial energies are needed in order to calculate the free energy and, more precisely, the first derivative of the free energy. A positive first derivative of the free energy indicates a stable thin layer of the deposited material on the substrate, otherwise the layer is unstable and collapses to droplets, particles or clusters. The gold on silicon oxide system is correctly predicted by the semi-empirical and empirical models. Only the fully theoretical model fails by predicting a stable thin gold layer on silicon oxide. One reason for this error is the unknown ratio of different oxide species on the substrate surface and their unknown orientation. This makes an exact theoretical description difficult. The two empirical models predict the formation of isolated droplets without a wetting layer in-between. The experiments with MBE formed gold droplets on silicon oxide show no material exchange between the droplets. The data indicate a re-evaporation process at elevated temperatures, which is due to a temperature induced reduction of Laplace pressure in the overall system.

The gold on silicon system is correctly predicted by all three models. The first derivative of the free energy indicates a droplet formation above 0.34 nm, which corresponds to a monolayer of gold. This means that an ultrathin layer of gold on silicon must be stable. This wetting layer can be considered as a mediating communication layer or also as a material transport layer, which enable Ostwald ripening processes. Indeed, the MBE formed gold droplets on silicon show material fluctuation between the droplets. Here, the increased Laplace pressure is not reduced by re-evaporation, but by Ostwald ripening, which requires a medium of material transport and has a lower activation energy than evaporation. The monolayer of gold between the droplets represents this medium. The contribution of the droplet diameters also indicates an Ostwald ripening process.

With the models shown here it is possible to predict the behaviour of droplets under consideration of free energy. This knowledge provides the understanding of dewetting

phenomena of thin metal layers and for the fabrication of nano- and microelectronic devices, such as energy conversion cells, FETs or thermoelectric materials by nanowires.

Experimental

Theory

The ability of a fluid to disperse or form droplets on a substrate is related to the free energy $\mathbf{F_{(d)}}$ of the system depending on the layer thickness d:

$$\frac{F_{(d)}}{A} = \frac{F_0}{A} + R_{(d^{-2})} - \Gamma \qquad (1)$$

where F_0 is the basic free energy, R is a contribution of van der Waals energy, Γ is the so-called spreading factor and **A** is the surface area.[27] Since R is a long-range force it decreases with the square of the film thickness $\mathbf{d^2}$ and increases proportionally with the difference between the Hamaker constants $\mathbf{A_{SF}}$ of solid-liquid and $\mathbf{A_{FF}}$ of fluid-fluid interaction:

$$R = \left(\frac{A_{SF} - A_{FF}}{12 \cdot \pi \cdot d^2}\right) \qquad (2)$$

The Hamaker constants are a scale for the interaction between particles of certain materials and the electric fields they generate.[28] This electrical responsiveness or susceptibility is closely related to the permittivity/polarizability α of the materials, the particle volume density m and the (first) ionization energies I of the particles:

$$A_{ij} = \frac{3}{2} \cdot \pi^2 \cdot \alpha_i \cdot \alpha_j \cdot m_i \cdot m_j \cdot \frac{(I_i \cdot I_j)}{(I_i + I_j)} \qquad (3)$$

It follows that a fluid layer can be attracted or repelled by a substrate, which leads to a wetting or dewetting tendency.

The spreading factor Γ is defined as the difference between the surface energy of the pristine substrate γ_S and the surface energies of the wetted substrate (γ_{SF}+γ_F):

$$\Gamma = \gamma_S - (\gamma_{SF} + \gamma_F) \quad (4)$$

In an ideal van der Waals system, it can be shown that surface energies are also associated with polarizability.[29] For real systems, however, it is more precise to use experimentally measured surface energies that are listed for many materials in the literature. Although, the determination of the surface energy between substrate and fluid, also called the interfacial energy γ_{SF}, can be more challenging. Thus the following three methods are used to determine and compare the respective interfacial energy: 1. Empirical by the wetting angle (**WA model**) 2. Fundamental by the long-distance contribution of the van der Waals energy (**vW model**) 3. Semi-empirical according to the Ewing model (**AE model**).

1. WA model: Determination of γ_{SF} by the droplet angle. In systems with droplet formation, the Young-Dupré equation[30][31][32] is used to determine the interfacial energy γ_{SF}. Since γ_{SF} is associated besides γ_S and γ_F with the contact wetting angle θ, the angle between substrate and drop surface has to be determined:

$$\gamma_{SF} = \gamma_S - \gamma_F \cdot \cos\theta \quad (5)$$

However, this equation is only valid for equilibrium states and on ideal surfaces. Defects on the substrate can lead to hysteresis effects that change the contact wetting angle.[33] Other surface effects such as coarsening, ageing or ripening can additionally lead to hysteresis effects that make it more complicated to interpret the results.[34]

2. vW model: Determination of γ_{SF} by the long range contribution of the van der Waals energy. As mentioned before, the surface energies are also connected with the polarizability of the system, i.e. with the Hamaker constants. In order to approximate the interfacial energy, it can be assumed that free surfaces with given Hamaker constants are brought closer together. If the surfaces reach a distance of the diameter

of one particle, the two surfaces touch each other. At this point, the non-retarded van-der-Waals interaction will match the ratio of surface energies. More precisely, the spreading factor Γ is the limit value of **R** at the point $\mathbf{d=d_0}$ with $\mathbf{d_0}$ as particle diameter[29]:

$$R_{(d_0)} = \left(\frac{A_{SF} - A_{FF}}{12 \cdot \pi \cdot d_0^2}\right) = \Gamma = \gamma_S - (\gamma_{SF} + \gamma_F) \quad (6)$$

Thus the interfacial energy can be determined by the **R**-value and the surface energies:

$$\gamma_{SF} = (\gamma_S - \gamma_F) - \left(\frac{A_{SF} - A_{FF}}{12 \cdot \pi \cdot {d_0}^2}\right) \quad (7)$$

3. AE model: Determination of γ_{SF} according to R. H. Ewing. The AE model offers a semi-empirical possibility to determine the interfacial energy γ_{SF}.[35] R. H. Ewing postulated that the interfacial energy of a solid material and its own melt consists of an energetic part of the solid γ_{SF}^{S} and a part of the fluid γ_{SF}^{F} because the chemical and physical bonds between the material and its melt are solid and liquid at the same time:

$$\gamma_{SF} = {\gamma_{SF}}^{S} + {\gamma_{SF}}^{F} \quad (8)$$

More information can be found at R. H. Ewing's publications.[36],[37] In the following, the model is not used to calculate the interfacial energy between a solid and its own melt, but instead, to determine the interfacial energy between a solid and a fluid of another compound. This results in a sufficient well approximation for the true value of γ_{SF}.

However, the wettability of a system is not directly predictable by the free energy itself, but by the slope of its function. Accordingly, this is given by the first derivative of free energy. In order to derive the free energy, a constant volume for the system with $A=V\times d$ must be considered. The three different descriptions for the interfacial energy result in:

WA model,

$$\frac{\partial \frac{\Delta F_{(d)}}{\Delta V}}{\partial d} = -\left(\frac{A_{SF} - A_{FF}}{4\pi d^4}\right) - \frac{\gamma_F(\cos\theta + 1)}{d^2} \quad (9)$$

vW model,

$$\frac{\partial \frac{\Delta F_{(d)}}{\Delta V}}{\partial d} = -\left(\frac{A_{SF} - A_{FF}}{4\pi d^4}\right) + \frac{A_{SF} - A_{FF}}{12\pi {d_0}^2 d^2} \quad (10)$$

AE model,

$$\frac{\partial \frac{\Delta F_{(d)}}{\Delta V}}{\partial d} = -\left(\frac{A_{SF} - A_{FF}}{4\pi d^4}\right) + \frac{\left(\gamma_S - ({\gamma_{SF}}^S + {\gamma_{SF}}^F + \gamma_F)\right)}{d^2} \quad (11)$$

If the first derivative is positive, then the fluid wets the substrate. At negative values, dewetting will occur. At zero, there is a stable maximum thickness and droplets form as soon as this thickness is exceeded. In this case, a material layer of the maximum stable thickness, the wetting layer, may persist between the droplets. However, all calculations shown here apply only to thicknesses below capillary length (>1µm) of the fluid, since gravity can be neglected within this range.[29]

Table (1) (Appendix) shows the set of values required for calculating the free energy per unit area and its first derivative for gold on silicon oxide and gold on silicon.

Experiments

The UHV-PVD experiments were carried out in a molecular beam epitaxy (MBE) chamber with a base pressure of 2×10^{-10} mbar. Two different types of substrates were used for the experiments: The first type of substrates are single-crystalline Si(111) wafers of 25×25×0.525 mm³ size which where chemically cleaned by the conventional RCA 1 and RCA 2 etching process to get hydrophilic silicon surfaces immediately before transferring to the UHV system. Before the growth, the Si(111) substrates were annealed at 900 °C for 30 min to desorb residual silicon oxide from the surface. The second variety of substrates consist of a chemical vapour deposited (CVD) SiO_x layer

(500 nm thick) on top of a Si(001) wafer. The subsequent chemical mechanical polishing provides a highly-flat-surface (RMS 0.3 nm). Gold with a nominal thickness of 1 nm was evaporated from an effusion cell onto the heated substrate with a deposition rate of 0.01 nm/s, which was calibrated before with an Inficon XTC/3 quartz crystal microbalance. Series of experiments were carried out at substrate temperatures of 300, 400, 500, 550, 600, and 650°C in case of SiO_x on Si(001) and substrate temperatures in the range of 400 to 700°C in steps of 50 K for Si(111) wafers. The gold droplet formation was analysed with a Dual Beam FEI Nova 600 NanoLab scanning electron microscope (SEM). The SEM images were used to determine the shapes, sizes, number and wetting angles of gold droplets. The growth of germanium structures took place at temperatures of 500 °C and germanium deposition rates of 0.005 $nm\,s^{-1}$. Since the solubility of germanium in gold is high, a supersaturated mixture will form. To reduce the supersaturation germanium may precipitate at the bottom of the gold droplet. This way germanium nanowires may grow. This process is known as vapour-liquid-solid-process (VLS).

Supporting information

Supporting information features all values used for the calculations shown in figure 1 and equations 9, 10, and 11 including their references.

File name: Appendix_Ernst er al_Analysis of catalyst surface wetting_the early stage of epitaxial germanium nanowire growth.docx

File format: word (.docx)

Title: Appendix

Acknowlegement

The authors sincerely thank Dr. Roman Bansen and Dr. Toni Markurt for TEM sample preparation and investigation.

References

1. Khanna, R.; Nigam, K. D. P. *Chem. Eng. Sci.* **2002**, *57* (16), 3401–3405

2. Seemann, R.; Brinkmann, M.; Pfohl, T.; Herminghaus, S. *Reports Prog. Phys.* **2012**, *75* (1), 016601

3. Zhang, J.; Tan, K. L.; Hong, G. D.; Yang, L. J.; Gong, H. Q. *J. Micromechanics Microengineering* **2001**, *11* (1), 20–26

4. Greener, J.; Li, W.; Ren, J.; Voicu, D.; Pakharenko, V.; Tang, T.; Kumacheva, E. *Lab Chip* **2010**, *10* (4), 522–524

5. Herminghaus, S.; Jacobs, K.; Mecke, K.; Bischof, J.; Fery, A.; Ibn-Elhaj, M.; Schlagowski, S. *Science (80-.).* **1998**, *282* (5390), 916 LP – 919

6. Leroy, F.; Borowik, Ł.; Cheynis, F.; Almadori, Y.; Curiotto, S.; Trautmann, M.; Barbé, J. C.; Müller, P. *Surf. Sci. Rep.* **2016**, *71* (2), 391–409

7. Baffou, G.; Polleux, J.; Rigneault, H.; Monneret, S. *J. Phys. Chem. C* **2014**, *118* (9), 4890–4898

8. Robert, H. M. L.; Savatier, J.; Vial, S.; Verghese, J.; Wattellier, B.; Rigneault, H.; Monneret, S.; Polleux, J.; Baffou, G. *Small* **2018**, *14* (32), 1801910

9. Wu, Y. Y.; Eizenberg, M. *Thin Solid Films* **2006**, *514* (1–2), 33–44

10. Kondati Natarajan, S.; Nies, C.-L.; Nolan, M. *J. Mater. Chem. C* **2019**, *7* (26), 7959–7973

11. Ringleb, F.; Andree, S.; Heidmann, B.; Bonse, J.; Eylers, K.; Ernst, O.; Boeck, T.; Schmid, M.; Krüger, J. *Beilstein J. Nanotechnol.* **2018**, *9*, 3025–3038

12. Schmidtbauer, J.; Bansen, R.; Heimburger, R.; Teubner, T.; Boeck, T. *J. Cryst. Growth* **2014**, *406*, 36–40

13. Yu, L.; O'Donnell, B.; Alet, P.-J.; Conesa-Boj, S.; Peiró, F.; Arbiol, J.; Cabarrocas, P. R. i. *Nanotechnology* **2009**, *20* (22), 225604

14. Kramer, A.; Boeck, T.; Schramm, P.; Fornari, R. *Phys. E Low-dimensional Syst. Nanostructures* **2008**, *40* (7), 2462–2467

15. Hu, G.; Edwards, H.; Lee, M. *Nat. Electron.* **2019**, *2* (7), 300–306

16. Filipovic, L.; Grasser, T. *Micromachines* **2019**, *10* (5)

17. Boukai, A. I.; Bunimovich, Y.; Tahir-Kheli, J.; Yu, J.-K.; Goddard, W. A.; Heath, J. R. Silicon Nanowires as Efficient Thermoelectric Materials. In *Materials for Sustainable Energy*; Co-Published with Macmillan Publishers Ltd, UK, 2010; pp 116–119

18. Swinkels, M. Y.; Zardo, I. *J. Phys. D. Appl. Phys.* **2018**, *51* (35), 353001

19. Gadea, G.; Pacios, M.; Morata, Á.; Tarancón, A. *J. Phys. D. Appl. Phys.* **2018**, *51* (42), 423001

20. Niu, G.; Capellini, G.; Schubert, M. A.; Niermann, T.; Zaumseil, P.; Katzer, J.; Krause, H.-M.; Skibitzki, O.; Lehmann, M.; Xie, Y.-H.; von Känel, H.; Schroeder, T. *Sci. Rep.* **2016**, *6* (1), 22709

21. Janssen, D.; De Palma, R.; Verlaak, S.; Heremans, P.; Dehaen, W. *Thin Solid Films* **2006**, *515* (4), 1433–1438

22. Geiger, F.; Busse, C. A.; Loehrke, R. I. *Int. J. Thermophys.* **1987**, *8* (4), 425–436

23. Voorhees, P. W. *J. Stat. Phys.* **1985**, *38* (1), 231–252

24. Lifshitz, I. M.; Slyozov, V. V. *J. Phys. Chem. Solids* **1961**, *19* (1–2), 35–50

25. Ressel, B.; Prince, K. C.; Heun, S.; Homma, Y. *J. Appl. Phys.* **2003**, *93* (7), 3886–3892

26. Kautz, J.; Copel, M. W.; Gordon, M. S.; Tromp, R. M.; van der Molen, S. J. *Phys. Rev. B* **2014**, *89* (3), 35416

27. Wyart, F. B.; Daillant, J. *Can. J. Phys.* **1990**, *68* (9), 1084–1088

28. Hamaker, H. C. *Physica* **1937**, *4* (10), 1058–1072

29. de Gennes, P. G. *Rev. Mod. Phys.* **1985**, *57* (3), 827–863

30. Young, T. *Philos. Trans. R. Soc. London* **1805**, *95*, 65–87

31. Dupré, P.; Dupré, A. *Théorie Mécanique de La Chaleur Capitre IX, Par M. Athanase Dupré,...[Partie Expérimentale En Commun Avec Paul Dupré.].*; Gauthier-Villars, 1869

32. Langmuir, I. *J. Chem. Phys.* **1933**, *1* (11), 756–776

33. de Jonghe, V.; Chatain, D. *Acta Metall. Mater.* **1995**, *43* (4), 1505–1515

34. Cassie, A. B. D. *Discuss. Faraday Soc.* **1948**, *3*, 11–16

35. Jones, H. *Mater. Lett.* **2002**, *53* (4–5), 364–366

36. Ewing, R. H. *J. Cryst. Growth* **1971**, *11* (3), 221–224

37. Ewing, R. H. *Philos. Mag. A J. Theor. Exp. Appl. Phys.* **1972**, *25* (4), 779–784